Published in final edited form as:
Chemistry. 2009 June 2; 15(23): 5749–5762. doi:10.1002/chem.200900280.

Step-wise Conversion of Two Pyrrole Moieties of Octaethylporphyrin to Pyridin-3-ones: Synthesis, Mass Spectral and Photophysical Properties of Mono- and Bis(oxypyri)porphyrins

Dr. Claudia Ryppa[a], **Dr. Dariusz Niedzwiedzki**[a], **Nicole L. Morozowich**[a], **Dr. Rapole Srikanth**[a], **Prof. Dr. Matthias Zeller**[b], **Prof. Dr. Harry A. Frank**[a], and **Prof. Dr. Christian Brückner**[a]

Christian Brückner: c.bruckner@uconn.edu

[a]Department of Chemistry, University of Connecticut, Unit 3060, Storrs, CT 06269-3060 (U.S.A.), Fax: (+1) 860 486 2743

[b]Department of Chemistry, Youngstown State University, One University Plaza, Youngstown, OH 44555-3663 (U.S.A.)

Abstract

Free base octaethylporphyrin (OEP) was converted, in two steps (β,β′-dihydroxylation, oxidative diol cleavage with concomitant aldol condensation), to the corresponding oxypyriporphyrin. This conversion was previously described to be only applicable to the Ni(II) complex of OEP. Modified diol cleavage conditions made this reaction sequence now applicable to free base OEP. The single crystal structure of the resulting free base oxypyriporphyrin was determined, proving its near-perfect planarity. The reaction sequence can also be applied to oxypyriporphyrin itself, generating the unprecedented bacteriochlorin-type bis-oxypyriporphyrin as two separable isomers. The ground state (UV/Vis and fluorescence) and excited state (transient triplet-triplet absorption, triplet lifetimes, and triplet EPR) photophysical properties of all chromophores are described and contrasted against OEP, chlorins, and oxochlorins. The pyridone-modified porphyrins possess unique spectroscopic signatures that distinguish them from regular porphyrins or chlorins. The presence of the pyridone moiety alters the ESI+ collision-induced fragmentation properties of these oxypyriporphyrins only to a minor degree when compared to those of OEP or chlorins, attesting to their stability.

Keywords

porphyrins; porphyrinoids; octaethylporphyrin; chlorins; photophysics; tandem mass spectrometry

Introduction

The chemical and physical properties of porphyrinic compounds in nature are adjusted by the variation of the degree of saturation of the tetrapyrrolic macrocycle, as in chlorins (2,3-dihydroporphyrins) or bacteriochlorins (2,3,12,13-tetrahydroporphyrins), or by variation of

Correspondence to: Christian Brückner, c.bruckner@uconn.edu.

CCDC-718691 (**12**) contains the supplementary crystallographic data for this paper. These data can be obtained free of charge from The Cambridge Crystallographic Data Centre via www.ccdc.cam.ac.uk/data_request/cif.

Supporting information for this article is available on the WWW under http://www.chemeurj.org/ or from the author.

the substituent pattern on the macrocycle periphery.[1] The latter may affect the porphyrinic π–system either directly through conjugation or indirectly through the tuning of the conformation of the macrocycle.[2]

Porphyrins and chlorins are attractive targets for use in a diverse range of technical and medicinal applications.[3] The majority of these applications requires the ability to tune their photophysical properties. While progress has been made in the understanding of the factors controlling the optical properties of porphyrins, much is left to be desired for the synthesis of porphyrins with designed physical and chemical properties. As a consequence, this area represents one of the foci in current porphyrin research.[4]

The search for porphyrins with tunable long wavelength absorbing and emitting properties led to the development of porphyrinic chromophores that have no natural precedent, including expanded porphyrins, porphyrin isomers, or porphyrin analogues that contain non-pyrrolic building blocks.[5–7] The bulk of these porphyrinoids are made by total synthesis, i.e., they are synthesized in one or more steps from mono-pyrrolic precursors.

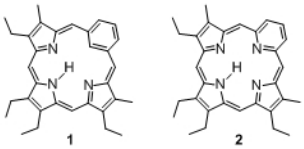

1 2

Examples of porphyrinoids containing non-pyrrolic building blocks are carbaporphyrins such as benziporphyrin **1**[7,8] or pyriporphyrin **2**.[9–12] However, the benzene and pyridine moieties, respectively, are not fully conjugated into a porphyrin-like aromatic system. In contrast, oxypyriporphyrin **3** contains a porphyrin-like π-aromatic system incorporating the pyridone moiety.[13–16] Lash and his group have optimized the 3+1 total synthesis approach toward oxybenziporphyrins and related macrocycles (Scheme 1).[6] A tripyrrane, such as **4** (often prepared *in situ)*, is condensed with a bisaldehyde, such as 2-formylsalicylaldehyde, and the intermediate macrocycle is aromatized by means of an oxidation. This pathway proved to be extremely successful and led to the synthesis of a wide structural variety of pyrrole-modified porphyrins and carbaporphyrins.[6]

A Fe-complex of oxypyriporphyrin was prepared and apomyoglobin reconstituted with this heme analogue.[17,18] The holoenzyme did not exhibit a measurable affinity for oxygen and exhibited a number of other functional anomalies when compared to native myoglobin, but provided valuable insight into the structural ligand control of oxygen binding and provided a model compound for one other heme enzyme, guanylate cyclase.

An alternative approach toward pyrrole-modified porphyrins is the modification of a readily available porphyrin, such as *meso*-tetraphenylporphyrin (TPP) or octaethylporphyrin (OEP, **5**, Scheme 2). The earliest example of a porphyrinoid resulting from an insertion reaction of a carbon into a pyrrolic unit of a porphyrin was reported by Callot and Schaeffer.[11,19] A Ni(II)-induced rearrangement of a *N*-substituted TPP resulted in the ring expansion of one of the pyrrole moieties to form azine-modified porphyrin **6**. Crossley and King reported a series of oxidation reactions of 2-amino-substituted TPP that lead to the observation of a series of pyrrole-modified porphyrins, among them anhydride **7**.[20]

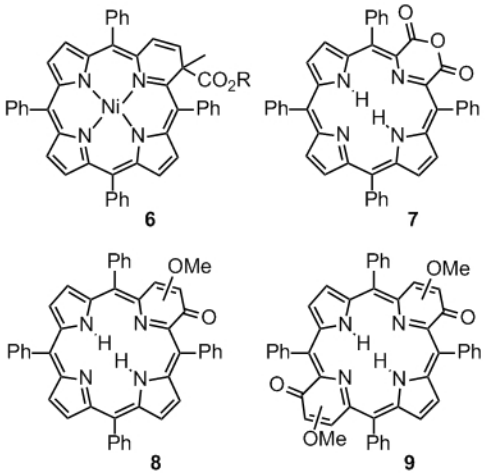

We reported the step-wise functionalization of TPP that leads to its conversion to, for instance, morpholino- or pyrazinochlorins and we demonstrated their unique properties as compared to, porphyrins and chlorins.[21] The one-step reaction of 2,3-dioxo-TPP and 2,3,12,13-tetraoxo-TPP[22] with diazomethane allowed the preparation of oxypyriporphyrin **8** and bis(oxypyri)porphyrin **9**, each prepared as mixtures of inseparable regioisomers.[23] Compound **9** is a rare examples of a bis-pyrrole-modified system.[24] It is, to our knowledge, the only porphyrinoid system containing two six-membered rings known to date.

Bonnett and co-workers firstly described the step-wise functionalization of OEP to form an octaalkyloxypyriporphyrin (Scheme 2).[27,28] OEP was first converted to 2,3-dihydroxychlorin **10**, followed by insertion of Ni(II) to form **10Ni** and a $Pb(IV)(acetate)_4$-induced diol cleavage reaction to form the Ni(II) complex of secochlorin **11Ni**. Under base catalysis, this diketone underwent an intramolecular aldol condensation, resulting in the formation of the oxypyriporphyrin Ni(II) complex **12Ni**.[27,28] Thus, one pyrrole unit in OEP was formally replaced by a six-membered pyridin-3-on moiety in two well controlled and efficient steps. The influence of this seminal paper on the development of strategies toward the conversion of porphyrins to other pyrrole-modified porphyrins cannot be underestimated and, as the forthcoming will reveal, this contribution is a direct extension of this work.

The potentially much more useful free base analogue to **12Ni** could not be prepared, however.[27,28] Demetalation of **12Ni** was unsuccessful and the oxidation of free base diol **10** resulted in a complex mixture from which no product could be isolated. Since the structurally very similar free base compound **3** and related compounds are stable when prepared by total synthesis,[15,16,29] the problem likely lies in the instability of the intermediate free base secochlorin **11**. Whereas its Ni(II) complex **11Ni** is stable and could be structurally characterized,[27,28] free base secochlorin **11** may not be stable enough under the reaction conditions employed to allow high-yielding conversions. This conclusion is mirrored by our own findings that Ni(II) imparts particular stability on TPP-derived secochlorins.[30,25]

To account for the limited stability of TPP-derived free base secochlorins and to circumvent the problem of removing Ni(II) from the final product, we devised two principle synthetic methodologies: one uses Ag(II) as a stabilizing but removable metal ion template,[31] the other is a two-step, one-pot approach in which the free base secochlorin, prepared *in situ* using mild diol cleavage conditions ($NaIO_4$ heterogenized on silica gel), is trapped with an appropriate reagent.[32]

The latter synthetic methodology was successfully tested. Thus, we report here the step-wise conversion of OEP, **5**, to free base pyrrole-modified porphyrin **12**. Moreover, the mild β,β′-cleavage and ring-fusion conditions allowed the preparation of two isomeric bis(oxypyri)porphyrins **16**, the first examples of their class. We further report the crystal structure of **12**, the ground (UV/Vis and fluorescence) and excited state (triplet spectra, triplet life times and EPR spectra) photophysical properties of all novel macrocycles, and their collision-induced fragmentation mass spectra. We contrast the results obtained to their non-pyrrole-modified counterparts. This allows the derivation of some structure-physical properties relationships for these porphyrinoids.

Results and Discussion

Diol cleavage of dihydroxychlorin 10 – synthesis of oxypyriporphyrin 12

Confirming the report by Bonnett,[27,28] oxidation of **10** with Pb(IV) acetate does not allow the isolation of any product in reasonable yield. We surmised that the Pb(IV)-acetate/THF reaction conditions are too acidic for secochlorin **11**. Thus, reaction of blue diolchlorin **10** with a slurry of $NaIO_4$-impregnated silica gel in $CHCl_3$ containing 1–10% Et_3N results in the formation of a less polar red-purple product (Scheme 3). Its ESI+ mass spectrum suggests the composition for the expected bisketone **11** (*m/z* = 567.3679 for $[\mathbf{11}\cdot H]^+$). The major fragment ion of this compound is $[MH - H_2O]^+$, perhaps indicating that an aldol condensation reaction of **11** to form **12** is taking place under the conditions of the ESI+ mass spectrometric measurement. However, the ^1H NMR spectrum of the red product shows in the chemical shift range typical for *meso*-protons, instead of the two signals expected, four singlets (at 10.46, 9.94, 9.88, and 9.80 ppm, corresponding to 1H each), and two non-equivalent NH protons. The ^{13}C NMR spectrum confirms the presence of a molecule lacking two-fold symmetry and indicates the presence of one carbonyl carbon (δ = 202.1 ppm in the ^{13}C NMR) in conjunction with two significantly low-field-shifted pyrrolidine-like sp^3-carbons (δ = 79.7 and 71.0 ppm). All together, the data suggests that diol cleavage of **10** to diketone **11** has taken place but that this diketone has reacted spontaneously to form aldol product **14**. Commensurate with this assignment, the Soret band in the UV/Vis spectrum is significantly more red-shifted (λ_{max} = 410 nm; Figure 1) compared to the spectrum for the starting diol chlorin **10**, but altogether very much different from that described for oxypyriporphyrin **3**.[15,16,29] This is likely an effect of the presence of the reduced 'β,β′-bond' in the dihydropyridone moiety. Compound **14** is not stable and significantly decomposes in solution within a day. The addition of base (up to 10 vol% DBU) or catalytic amounts of acid (TFA fumes) hastens its disappearance but leads cleanly to the appearance of a bright green product with an *m/z* ratio of 548.3533 in its ESI+ spectrum, corresponding to $C_{36}H_{45}N_4O + H^+$, the composition expected for the target free base aldol condensation product oxypyriporphyrin **12**.

These findings suggested the use of DBU as base for a one-pot, two-step conversion of free base diolchlorin **10** to oxypyriporphyrin **12**. Indeed, addition of free base diolchlorin **10** to a slurry of the silica gel/$NaIO_4$ oxidant in $CHCl_3$ in the presence of 5–10 vol% DBU leads, over the course of 2 to 12 h at ambient temperature, to a conversion of the initially blue solution to a green solution. TLC analysis revealed the formation of one major bright green compound of lesser polarity. This product can be, after chromatographic separation and crystallization, isolated in over 50% yield (at up to 1×10^{-4} mol scales) as a purple microcrystalline solid, and proved to be identical to oxypyriporphyrin **12** described above (Scheme 3). Of all the bases tested (pyrazole and imidazole – no conversions; pyridine and Et_3N – slow conversion) we found DBU to be the best base to cleanly and rapidly lead to the formation of the product.

When compared to the spectrum of diol chlorin **10**, the chromophore is blue-shifted and more porphyrin-like (Figure 4). As expected, the UV/Vis spectrum of the product is near-identical to that of oxypyriporphyrin **3**.[15] A discussion of the UV/Vis spectra of this and the other novel compounds prepared herein is presented below. Also, we will detail the ESI+ collision-induced fragmentation spectra of **12** and other novel compounds below.

The ^{1}H NMR spectrum of oxypyriporphyrin **12** shows the diagnostic peaks described for this compound class,[15,16,29] modulated by the particular substitution pattern present: next to the four low-field signals assigned to the non-equivalent *meso*-protons, two high-field signals assigned to the NH protons can be distinguished. One methyl group (s at 2.82 ppm, 3H) can also be differentiated; the remaining ethyl groups show significant overlaps. The combination of HMQC, HMBC and NOESY spectra allowed the unambiguous assignment of most peaks in the ^{1}H and ^{13}C NMR spectra. In summary, the spectroscopic properties of this compound unambiguously identify it as free base oxypyriporphyrin **12**. It thus expands the number of known derivatives of this compound class,[15,16,29] but more importantly, it demonstrates the applicability of the porphyrin β,β′-bond cleavage and ring-fusion strategy toward the synthesis of free base OEP-derived pyrrole-modified porphyrins.

Standard Zn(II) insertion protocols generate the complex **12Zn**. This derivative also possesses the spectroscopic properties one would expect when projecting the data reported by Lash for similar complexes,[15] including its peculiar solubility and solvochromic properties that point toward extensive aggregation behavior (see SI).[33]

Single crystal X-ray structure of oxypyriporphyrin 12

The spectroscopically derived connectivity of **12** could be confirmed by single crystal X-ray crystallography, the first example of a structural characterization of this class of pyrrole-modified porphyrins (Figure 2A). Somewhat surprising is the pronounced planarity of the oxypyriporphyrin chromophore (Figure 2B). Evidently, the expansion of a pyrrolic moiety by a carbonyl group is readily absorbed by the macrocycle without causing any major distortions. In comparison, the related free base pyriporphyrins, such as **2**, are expected to be decidedly non-planar, with the mean plane of the pyridine moiety taking up a steep angle with respect to the mean plane of the remaining tripyrrolic moiety, a feature that is even preserved in their metal complexes.[9,34]

Figure 3 illustrates the bond length and inner core distance differences observed in **12** with respect to the metrics of OEP.[35] The differences in the pyridone moiety are likely the result of the fixed enone conjugation of this cross-conjugated moiety. The additive effects of many small changes in the bond distances and angles (not shown) lead to a significant tetragonal distortion of the inner core of **12**. In OEP, the distances between opposing inner nitrogens are 4.052 (*N*-*N*) and 4.195 Å (*N*H-*N*H), respectively, i.e. the cavity is about 0.14 Å longer than wide, with the NH hydrogens positioned on the longer axis. In **12**, the cavity is significantly longer (4.326 Å, *N*-*N*) and slightly narrower (4.155 Å, *N*H-*N*H), but with the NH protons lying on the shorter axis. This elongation was recently predicted for the Fe(III) complex of an oxypyriporphyrin based on EPR data and quantum chemical calculations.[18]

Dihydroxylation of oxypyriporphyrin 12

The ability to formally replace one pyrrolic building block of free base OEP by a pyridin-3-one moiety in two reasonably high yielding reaction steps allows us to test whether this reaction sequence can be performed twice on OEP, giving rise to novel doubly pyrrole-modified chromophores. Two reaction pathways are perceivable: Firstly, an additional dihydroxylation of oxypyriporphyrin **12**, followed by diol cleavage/aldol reaction and,

secondly, the onestep, double diol cleavage/aldol reaction on known tetraolbacteriochlorins **17** (Scheme 2). Both approaches proved successful and each has its own merits.

Reacting green **12** with stoichiometric amounts of OsO_4 in $CHCl_3$/pyridine leads, over the course of one week, to the formation of one major, forest-green, polar product. Quenching of the osmate ester with H_2S, followed by chromatography and recrystallization, leads to the formation of a dark-green microcrystalline compound in acceptable yields (58%, 10^{-4} mol scale). High resolution ESI+ mass spectrometry confirms the composition of the product to be $C_{36}H_{47}N_4O_3$, i.e. the expected composition of the (protonated) diol adduct **15**.

It has been well established that OsO_4 adds to the double bond that leads to the smallest loss in resonance energy.[36] In porphyrins specifically, it attacks the double bond of largest olefinic character. Hence, at least two locations for the diol functionality are perceivable. Lash has shown that oxypyriporphyrins are aromatic, with an implied chlorin-like conjugation pathway.[15] Following the known directing effects of free base chlorins with respect to a second reduction or dihydroxylation,[37,38,39] we can expect the β,β′-double bond opposite to the oxypyridine moiety (C12-C13) to be the most likely dihydroxylation site, thus rendering the two β,β′-double bonds adjacent to the non-pyrrolic building block (either C7-C8 or C17-C18) as the less likely sites. On the other hand, we cannot exclude the enone functionality (C3-C2a double bond) in the pyridone moiety as a potential dihydroxylation site.[40]

Dihydroxylation of the pyridone moiety in **12** would generate a chromophore that is predicted to possess similar optical properties to **14**. Inspection of the UV/Vis spectrum of the bright-green compound, however, shows a much red-shifted spectrum compared to that of **14** ($\Delta\lambda_{max}$ of the longest wavelength band = + 23 nm), with the longest wavelength absorbance also being the most intense of all Q-bands (Figures 1 and 4). These changes in the UV/Vis upon dihydroxylation of **12** are suggestive of a β,β′-bond dihydroxylation forming 12,13-dihydroxyoxypyrichlorin **15**.

The diagnostic resonances in the ^{1}H NMR of **15** for the pyridone moiety are preserved and new signals indicative for a dihydroxy-pyrrolidine moiety appeared. If hydroxylation of a β,β′-bond adjacent to the pyridone moiety would have taken place, it would have generated a mixture of two regioisomers (each present as a racemic mixture), but we could not find any indication for the formation of any regioisomers. Diol **15** is expected to be a simple racemic mixture. Taken all together, the NMR data support the formation of bacteriochlorin-like **15**. As we will show below, definitive proof for this assignment is provided by the reaction products of **15**.

Diol cleavage of dihydroxyoxypyrichlorin 15 – synthesis of bis(oxypyri)porphyrins 16

Reaction of dihydroxyoxypyriporphyrin **15** with silica/$NaIO_4$ in $CHCl_3$/10% DBU at ambient temperature leads, over the course of ~2 h, to the formation of two less polar compounds (R_f-**16a** = 0.43, R_f-**16b** = 0.34, silica-$CHCl_3$/1% MeOH) in an 1:1 ratio. Their UV/Vis spectra are similar (Figure 4). Both possess identical compositions as determined by HR ESI+ mass spectrometry ($M+H^+$ corresponding to $C_{36}H_{43}N_4O_2$). The ^{13}C NMR spectra of **16a** and **16b** suggest the presence of two similar two-fold symmetric molecules: each possess only two signals assigned to *meso*-carbons (186.0, 152.4 and 185.6, 152.5 ppm, respectively), one methyl signal (2.74 and 2.72 ppm, respectively), and one carbonyl carbon (186.0 and 185.6 ppm, respectively). Both compounds also possess different IR spectra (Figures S28 and S29). These data are as expected for the two isomeric bis(oxypyri)porphyrins **16a** and **16b** (Scheme 3). The identity of each isomer can be unambiguously assigned. One diagnostic feature in their ^{1}H NMR spectra are the number of NH signals. While the two NH groups in C_{2v}-symmetric **16a** are non-equivalent and show

two signals (br s at −4.40 and −4.45 ppm, 1H each), both NH groups are symmetry-equivalent in the C_{2h}-symmetric isomer **16b**, and only one signal can be distinguished (br s at −3.80 ppm, 2H).

Some of the NMR-derived symmetry arguments brought forward in support of the bacteriochlorin-type connectivity of chromophores **16a**/**b** can also be made for an isobacteriochlorin-like substitution pattern. However, such an isobacteriochlorin-type substitution pattern for **15** would have led to formation of three isomeric bis(oxypyri)porphyrins in an (idealized) 1:2:1 ratio. But most convincingly, the double oxidation of a genuine bacteriochlorin, tetraol **17**, also produced **16a**/**b**.

Diol cleavage of tetrahydroxybacteriochlorins 17 – alternate synthesis of bis(oxypyri)porphyrins 16

A one-pot, four-step conversion of tetraolbacteriochlorin **17** proved to be an alternate synthesis of bis(oxypyri)porphyrins **16a**/**b**. Thus, subjecting tetraol **17** to the standard diol cleavage reaction conditions, the pink solution turns green within 2 h at room temperature. Once TLC analysis of the reaction mixture has indicated the consumption of the tetraolbacteriochlorin, three products can be identified: The mono-oxidized compound **15** – thus establishing the bacteriochlorin-type substitution pattern of this compound – and the two isomers of **16** in a ~1:1 ratio. Lengthening of the reaction time or addition of more oxidant converts the majority of **15** into **16a**/**b**, isolable in a combined yield of about 50%. While this reaction is simpler than the stepwise approach, the preparation and purification of the tetraols **17** are more tedious than that of diol **10**, largely canceling the advantages of the simplicity of the final step.

Both stereoisomers of **17** (resulting from the two possible relative orientations of the *vic* diols with respect to each other – *syn* and *anti*) form identical sets of bis(oxypyri)porphyrins **16a**/**b** but for sake of simplicity, we generally used mixtures of the isomers of **17** in these reactions.

Absorption and fluorescence spectroscopy of singlet-states

We will be discussing the optical properties of the oxypyri-modified chromophores **12**, **15**, and **16a/b** in comparison to those of the parent porphyrin **5**, a typical chlorin, **10**, and a bacteriochlorin, **17**. To assess the influence of a carbonyl group, we also included known oxochlorin **18** in the comparison, made by a pinacol-pinacolone rearrangement of diol **10** (Scheme 2).[41] Focus in this comparison is the question in as far the pyridone-modified chromophores possess optical properties that are porphyrin- or chlorin-like or whether they are altogether unique.

Inspection of the UV/Vis spectra shown in Figure 4 reveals that the Q-bands in the UV/Vis spectrum of oxypyriporphyrin **12** are not at all chlorin-like. They are porphyrin-like with respect to their descending intensity with longer wavelengths, and the small intensity ratio of Q-bands to Soret band. This was noted before.[15,16,29] Likewise, bis-modified systems **16** are not chlorin or bacteriochlorin-like (cf. to **10** or **17**). The Soret band of **12** is, compared to porphyrin **5** or chlorin **10**, 25 and 32 nm red-shifted, respectively, and split. The latter feature is shared, albeit expressed to different degrees, by all pyridone-modified chromophores (**12**, **15**, **16**). Generalized, the effect of the presence of pyridone units merely results in a ~25 nm shift per unit of the Soret and side bands. Thus, removal of a β,β′-double bond in ‘porphyrin’ **12** to its 12,13-dihydroxyderivative **15** generates a chromophore that is equivalent to a 25 nm red-shifted 12,13-dihydroxychlorin, such as **10**.

The absorption spectrum of oxochlorin **18** is chlorin-like. Therefore, the presence of a conjugated ketone alone cannot account for the unexpected behavior of the oxypyri-systems and, therefore, it must be the combination of the presence of the six-membered ring composed of sp^2 carbons and the conjugated ketone. Removal of the pyridone C-C double bond, as in **14**, results in a chlorin-type spectrum (cf. to Figure 1).

The high extinction coefficients for **12** (log ε for λ_{Soret} = 5.14), support the notion that **12** is also essentially planar in solution, excluding conformational effects as primarily responsible for the modulation of the optical spectra. Of note is also the observation that the two regioisomers of the bis-modified systems **16a**/**b** have distinct, if similar, absorption and emission spectra.

The fluorescence emission spectra of the chromophores also show a signature feature for the presence of a pyridone moiety (in the absence of any other pyrrole modification), in that the second vibronic band possesses higher intensity than the (0-0) emission (Figure 4). This is not typically observed for porphyrins or chlorins. In the hybrid molecule **15**, the (red-shifted) chlorin character prevails. A possible practical advantage of the high intensity second vibronic band in the pyridone-modified systems **12** and **16** are the large separations between suitable long wavelengths of excitation and the highest intensity emission wavelengths. Otherwise, the porphyrin-typical small Stoke's shifts for the (0-0) band are observed in all systems. Moreover, the $\lambda_{max\text{-}emission}$ for **16a**/**b** are significantly red-shifted compared to those of mono-pyridone **12** or even bacteriochlorin **17**, though combined with similar, or even blue-shifted $\lambda_{max\text{-}absorption}$. Thus, the pyridone moieties introduce unique optical features into the porphyrinoid chromophore.

Base properties

Monoprotonation of the inner imine-type nitrogens of a regular porphyrin such as OEP distorts it from planarity, exposing its second imine-type nitrogen and making the second protonation to occur more readily than the first ($pK_{b1} < pK_{b2}$). Hence, the monoprotonated species is never observed and a spectrophotometric titration of OEP with TFA in CH_2Cl_2 exhibits sharp isosbestic points (Figure S17). In contrast, and confirming observations made by Lash,[15,16,29] the corresponding titrations of **12** or **16a**/**b** indicate step-wise protonation events (Figures S18–23). Step-wise addition of 1 equiv TFA to a solution of **12** in $CDCl_3$ shows the presence of only three NH protons (at −0.8, −1.2, and −2.7 ppm at ~0.1% TFA; see Figure S22). Aside from the high-field shift of a pair of methylene signals assigned to the 12^1,13^1-CH_2 groups and a high-field shift of the *meso*-protons, except the one signal assigned to 20-C*H*, no other major changes are observed. This indicates that only relatively minor conformational changes have taken place upon monoprotonation. This is consistent with the assumption that the pyrrole moiety opposite of the pyridone moiety is protonated. Given that the pyridone nitrogen is in conjugation with the carbonyl group, its basicity is also expected to be greatly diminished.

Triplet lifetimes

The triplet lifetimes, determined by the observation of the dynamics of the transient triplet-triplet absorption profiles (Figure S16), show a clear trend (Figure 4). The most symmetric, rigid chromophore that does not carry a conjugated ketone functionality, porphyrin **5**, has a lifetime of 530 μs.[42] The lifetime of the corresponding more flexible chlorin is about half this value (270 μs). The effects of the introduction of a second pyrrolidine moiety, as in bacteriochlorin **17**, is additive and its presence once again about halves the lifetime (110 μs). A conjugated ketone moiety, as in oxochlorin **18**, induces a lesser lifetime reduction (360 μs) compared to a pyrrolidine or a pyridone (**12**, 260 μs). Thus, both the introduction of a pyridone or pyrrolidine moiety have the same net effect. However, the effects of an

introduction of a second pyridone (as in **16**) or a pyrrolidine (as in **17**) to a framework already incorporating a pyridone are not linear; instead, a much more dramatic reduction of the lifetimes is observed, ranging from 46 to 32 μs.

The rate constant of intersystem crossing (k_{isc}) from the triplet state of π-systems to the ground singlet state is largely governed by non-radiative processes and can be expressed as:

$$k_{isc}(T_1^i \rightarrow S_{0v}) = \frac{2\pi}{\hbar} \left| \left\langle T_1^i \left| \widehat{H}_{\text{int}} \right| S_{0v} \right\rangle \right| \rho(E) \quad \text{(Eq. 1)}$$

Here, *i* indicates triplet state spin sublevel, H_{int} is the perturbation operator responsible for driving the population from the triplet (T_1) state to the isoenergetic vibrational level of the singlet ground state (S_{0v}), and $\rho(E)$ is the density of final states into which *isc* proceeds. The energy gap rule is expected to hold for $T_1 \rightarrow S_0$ transitions. Thus, a direct relationship between the energy of T_1 and its lifetime should be observed; the lower the T_1 energy, the shorter a lifetime can be expected. The difficulty in rationalizing the observed triplet lifetimes is the lack of phosphorescence data as a measure of the T_1 energy levels.

In general, the energy of the first excited triplet state is determined by the singlet-triplet splitting.[43] Assuming that this splitting is approximately the same for all molecules studied here, the order of the excited triplet state energies is expected to be the same as for their first excited singlet states. If this is correct, the shortest lifetimes for the first excited triplet state T_1 are expected for bacteriochlorin **17** and **16a**/**b**. While these chromophores indeed possess short lifetimes, chlorin-pyridone-hybrid **15** is also characterized by a very short lifetime τ without a concomitant very red-shifted $\lambda_{\text{max-absorption}}$. Thus, molecular structure also plays an important role in driving the $T_1 \rightarrow S_0$ transition. Ketones possessing nπ* T_1 states accelerate *isc* due to strong spin-orbit coupling with the low-lying ππ* states.[43,44] This rationalizes why the chromophores undergoing the fastest $T_1 \rightarrow S_0$ crossing are substituted by (multiple) ketone groups (like **16a**/**b**). It is important to note, however, that the presence of a ketone alone (as in oxochlorin **18**) is not sufficient to induce fast relaxation. Thus, the combination of π-extended chromophore, likely larger conformational flexibility of the bis-pyrrole modified compounds, and the presence of a (conjugated) ketone are required to rationalize the observed triplet lifetime trends. Again, this clearly differentiates the electronic structures of pyridone-modified systems from those of traditional porphyrins and chlorins.

Triplet-state EPR spectroscopy

A triplet state is, by definition, characterized by three-fold degeneracy due to three possible alignments of two unpaired electron spins. In absence of an external magnetic field, the spin-spin interactions in organic molecules have anisotropic character, leading to quantization along the principal magnetic axes system. The separation of the triplet T_x, T_y, T_z sublevels in absence of an external magnetic field is termed zero field splitting. Applying an external magnetic field provides the experimental possibility of switching the spin coupling from the internal molecular frame to a new frame quantized along the external magnetic field. Increase of the external magnetic field will increase the energy separation between triplet sublevels. EPR spectroscopy at liquid He temperatures allows the measurement of the transitions between magnetic triplet sublevels. The spin system can be described by a spin Hamiltonian. Proper treatment of this Hamiltonian allows the extraction of a number of factors that characterize the EPR spectrum and that allow conclusions to be made regarding the structural features of the chromophore.[45–47]

Among these measurables are the zero field splitting parameters *E* and *D*. The *D*-parameter defines the overall spatial extent of the triplet spin distribution. The *E* parameter describes the degree of in-planar asymmetry of the triplet state. The quantity $3|E|/|D|$, termed rhombicity, lies in the range between 0 and 1. For $E = 0$, the molecules posses a fully symmetrical (axial) distribution of the triplet spin, typical for molecules with 3-fold or higher axial symmetry. $3|E|/|D| = 1$ is characteristic for molecules with lower, orthorhombic symmetry.[45,48] Furthermore, the average inter-electron distance can be estimated, providing an estimate of the size of the triplet orbital.

The photoexcited triplet EPR spectra for oxypyriporphyrin **12** and its diol derivative **15** in comparison to porphyrin **5**, diol chlorin **10**, and oxochlorin **18** are shown in Figure 5. The *D* and *E* parameters and related values are collected in Table 1.

The line shape of the EPR spectrum of randomly oriented molecules in an excited triplet state is represented by a first derivative spectrum, generally possessing six resonances, two for every *x, y, z* canonical Cartesian axis of the external applied magnetic field (field parallel to principal molecular axis). The absolute magnitude of *D* and *E* parameters can be directly obtained from the spectral traces, assuming $2|D|$ for the splitting between the outmost lines, $|D| + 3|E|$ for splitting between intermediate lines and $|D| - 3|E|$ for splitting between the innermost lines (Figure 5). For $|E| \approx 0$ the intermediate and innermost resonances degenerate, and only four lines are observable in the EPR spectrum.[49]

The EPR spectrum of the parent porphyrins OEP, **5**, has four resonance signals (two of them are weak and appear at the fringes of the spectrum).[49] This line shape is characteristic for triplet state spin system with $|E| \approx 0$, and a $|D|$ parameter value of 0.0495 cm^{-1}, the largest number for all measured molecules. OEP possesses low orthorhombic (D_{2h}) symmetry due to the presence of the inner NH hydrogens. However, a value of $E \approx 0$ is clear evidence that their influence on the electron distribution in the **π**-chromophore is negligible. The average inter-electron distance between interacting spins is 2.72 Å.

The compounds **10**, **12**, **15**, and **18** of lesser symmetry all possess six resonance lines. Their *D*-parameter values are notably smaller and range from 0.0370 to 0.0399 cm^{-1}. Their lower symmetries are also evident in their non-zero *E*-parameters. The rhombocity varies from 0.50 to 0.66. The average inter-electron distance between spins is slightly larger compared to OEP, **5**, and range from 2.92 – 3.00 Å. This indicates that the triplet state electron density is less condensed for molecules with modified pyrrole rings. It suggests also that the triplet state has expanded to include ring substitutents possessing free electron pairs, such as the ketone functionalities.

Another characteristic property of EPR triplet state spectra is their polarization pattern. At low temperatures, the T_1 lifetime is shorter than the spin lattice relaxation between two spin alignment patterns of each triplet state T_x, T_y, T_z sublevel. Thus, a non-Boltzman occupation of the triplet manifold results. Observed transitions may be absorptive (*a*) or emissive (*e*). Interpretation of a particular polarization pattern observed can furnish information about intersystem crossing, spin dynamics and relaxation.[48,50,51]

Porphyrin **5** possesses an *aa/aa* polarization pattern, molecule **12** *aea/eae*, **10** *aea/eaa*, **18** *aaa/eaa* and **15** *aea/eaa*. Only oxypyriporphyrin **12** possesses the polarization pattern typical for free-base porphyrin macrocycles.[51,52] However, on the basis of structure and optical spectroscopic properties it possesses neither porphyrin nor chlorin symmetry. The other molecules have different and unique polarization patterns, reflecting their unique population of spin sublevels in the intersystem crossing process from S_1 state. Again, this clearly differentiates these chromophores from regular porphyrins and chlorins.

Tandem ESI(+) mass spectrometry

We, and others, reported previously ESI mass spectrometry investigations of porphyrins that revealed that their fragmentation patterns were diagnostic for the presence of certain functional groups and, in some cases, the observed fragmentation patterns were reflecting their solution state chemistry.[53],[54] Lash already noted a small peak in the EI mass spectrum of **3** corresponding to the loss of CO.[29] Is this presumed ring contraction reaction of the oxypyriporphyrins a common and general fragmentation pattern for oxypyriporphyrins under ESI(+) conditions, and might this be an indication of the relative stability of the oxypyriporphyrins compared to porphyrins? To answer these and other questions, we investigated the collision-induced fragmentation spectra of the pyridone-derived porphyrinoids **12**, **15**, and **16a** and **16b**, and compared them to those obtained for OEP, **5**, diol chlorin **10**, and oxochlorin **18**.

In general, the ESI(+) spectra of all chromophores investigated show primarily the MH^+ signal, and, as commonly observed under ESI conditions, no or only minor fragmentations are observed. However, the collision-induced fragmentation spectra (MS^2 spectra) of the MH^+ ions show rich fragmentation patterns (Figure 6).

The porphyrin OEP, **5**, shows the consecutive loss of at least five single carbon fragments (largely CH_4, and CH_3 units), all of which are solely attributed to the degradation of the β-ethyl groups. Diol chlorin **10** shows a similar pattern as **5**, modified by the loss of H_2O and, eventually, both oxygens. Of interest is that the peak corresponding to the loss of water (*m/z* = 551.3866) is, against expectations, and irrespective of the collision energy used, always of very low abundance.

Oxochlorin **18** possesses the same composition as this fragment ion at *m/z* = 551.3866; in fact, **18** was prepared by dehydration of **10**. But do both species possess the same structure? Indeed, the MS^3 spectra of both peaks are identical (not shown). Hence, an explanation for the low abundance of the $[M - H_2O + H]^+$ peak in the MS^2 spectrum of **10** likely lies in the fact that the loss of water implies that a pinacol-pinacolone-type rearrangement has to take place that, evidently, is not a facile reaction in the absence of a solvent matrix. The result also demonstrates that any exocyclic loss of water is of even higher energy.

The MS^2 spectrum of **18** shows no loss of CO (or any other oxygen containing species) but instead again the loss of a number of single carbon fragments, with the most abundant fragment being that corresponding to $[M - C_3H_8 + H]^+$ at *m/z* = 507.3178. The loss of C_3H_8 (44 amu) is observed in all compounds investigated, safe for the diol derivatives **10** and **15**, and in all cases it a very prominent fragment. We speculate that this is due to the degradation of two adjacent β-ethyl groups (**I**) to form a β,β′-fused cyclopropane moiety (**II**) (Scheme 4). This ring fusion is surprising but appears to us to be more reasonable than the alternative diradical structure **III**. Aside from a report on the formation of a cyclopropane fused to a chlorin,[55] this ring fusion has not been observed in porphyrins.

The MS^2 spectrum of oxypyriporphyrin **12** shows the now familiar one carbon fragment fragmentation pattern typical for β-octaethyl porphyrinoids. Only one of the major fragments can be associated with the loss of oxygen (in the form of CO), following the loss of C_3H_8. Hence, the CO loss is only a minor fragmentation pathway for **12** under tandem ESI(+) mass spectrometry conditions, a finding also confirmed by the MS^2 spectra of **15** – most similar to that of diol **10** – and of bisoxypyriporphyrin **16a** – very similar to that of the mono-oxypyriporphyrin **12**. The spectrum of **16b** (not shown) is identical to that of **16a**. Overall the results attest to the porphyrin-like stability of the planar and fully conjugated oxypyriporphyrins.

Conclusion

We have shown that a formal replacement of a pyrrolic building block in free base OEP by a pyridin-3-one moiety via step-wise derivatization is possible. The synthetic methodology used – dihydroxylation, followed by diol cleavage and aldol condensation of the resulting secochlorin *in situ* – produces a oxypyriporphyrin that is complementary to the compounds prepared by total syntheses.[15,16,29] We thus fill the gap between the total syntheses of the free base forms of these chromophores by Lash and the conversion of the Ni(II) complex of OEP to yield the [oxypyriporphyrinato]Ni(II) complexes featured by Bonnett.[27,28]

Surprising in its extent, the near-perfect planarity of free base oxypyriporphyrin **12** was shown by single crystal diffractometry. Compared to OEP, a small tetragonal distortion of the central cavity was noted. The doubly-modified systems, hitherto not accessible through total synthesis approaches, are readily accessible in regioisomerically pure forms. The photophysical properties of oxypyriporphyrins are characteristically different from both porphyrin or chlorins, whereby we surmise the combination of a π-conjugated ketone group and peripheral β,β′-like double bond are responsible for the observed effects. The expansion of the porphyrinic chromophore by a six-membered ring may also influence conformational flexibility. Collision-induced fragmentation mass spectra have demonstrated the minute effect that the presence of the pyridone moiety has on the gas-phase fragmentation properties of this class of chromophores. We interpret this fining as an indication of their porphyrin-like stability.

In summary, the results shed further light on the structure-physical properties and structure-chemical properties relationships of pyrrole-modified porphyrins. The straightforward syntheses of oxypyriporphyrin derivatives, combined with their stability and unique optical properties, invites their further study.

Experimental Section

General

^{1}H NMR and ^{13}C NMR spectra, recorded on Bruker instruments, were referenced to residual solvent peaks. All peak assignments listed were based on HMQC, NOESY, and HMBC spectra. IR spectra were recorded on a JASCO FT-IR-410 using a diffuse reflectance attachment (all IR spectra are shown in the SI). Elemental analyses were provided by Numega Resonance Labs Inc., San Diego, CA, U.S.A. The analytical TLC plates were aluminium backed Silicycle ultra pure silica gel 60, 250 mm; preparative TLC plates (20 × 20 cm, silica gel on glass) and the flash column silica gel (standard grade, 60Å, 32–63 μm) used were provided by Sorbent Technologies, Atlanta, GA, U.S.A.

Reagents

All reagents were used as received. Octaethylporphyrin[56] was provided by D. Dolphin, University of British Columbia, Canada. 2,3-Dihydroxy-octaethylchlorin (**10**), 2,3,12,13-tetrahydroxyoctaethylbacteriochlorin (**17**), 2-oxo-3,3,7,8,12,13,17,18-octaethylporphyrin (**18**)[25], and the silica-bound $NaIO_4$[57] were prepared as described previously. In a variation of the literature procedures, we found it advantageous to chromatograph the osmate esters of **10** and **17** (silica - $CHCl_3$ with a gradient of 1 to 3% MeOH), instead of the diol or tetraols, respectively. Once the respective esters were separated, they were treated with H_2S to liberate the target compounds.

Mass Spectrometry

Mass spectral analysis were performed on a quadrupole time-of-flight (Q-TOF) mass spectrometer (QSTAR Elite) and a 4000 QTrap hybrid triple quadrupole linear ion trap mass spectrometer (both Applied Biosystems/MDS Sciex, Foster City, CA, USA), both equipped with an ESI sources. The data acquisition was under the control of the Analyst QS software (Foster City, CA). All samples were dissolved in spectral grade CH_3CN to achieve a final concentration of 10–20 μM. For either instrument, samples were infused into the ESI source at a flow rate of 10 $\mu L \cdot min^{-1}$ (either using from a build-in or Harvard Apparatus syringe pump). Typical source conditions for the Q-Star were: Capillary voltage, 5500 V; declustering potential, 80 V; focusing potential, 280 V; declustering potential 2, 15 V; resolution 15,000 (full-width half-maximum). Ultra high pure N_2 was used as the nebulizer, curtain and collision gas. For the CID experiments, the precursor ion was selected using the quadrupole analyzer and the product ions were analyzed using the TOF analyzer. Collision energies between 50–65 V were used. For QTrap mass spectral analysis, the turboionspray ion source conditions were optimized and set as: Curtain gas, 10; collision gas, high; ionspray voltage, 5500 V; ion source gas 1, 12; declustering potential, 30 V. Nebulizer and collision gas was N_2. The most abundant product ions in the MS/MS (MS^2) were also subjected to MS/MS/MS (MS^3) experiments.

UV/Vis and Fluorescence Spectroscopy

Absorption spectra were recorded using a Varian Cary 50 UV/Vis spectrophotometer in toluene at ambient temperature. The fluorescence spectra were recorded in the same solvent on a Cary Eclipse instrument with $\lambda_{excitation} = \lambda_{Soret}$.

Transient Triplet-Triplet Absorption Spectra and Triplet Lifetime Measurements

Samples were dissolved to OD = 1.5 at their respective λ_{Soret} in either toluene (Fisher HPLC grade) or 2-methyltetrahydrofuran (2-MTHF, Sigma-Aldrich 99+%) in a 1.00 cm cuvette fitted with a vacuum adapter. Every sample was degassed by means of at least 6 freeze-pump-thaw cycles. Samples were kept under vacuum during the measurements. The experiments were performed at room temperature with excitation from a Quanta-Ray Pro-230/MOPO-710 Nd:YAG laser system having a pulse repetition rate of 9.8 Hz and an output energy of ~9 mJ. The laser beam was focused onto the sample at a right angle to the measuring beam which consisted of an Oriel 150 W Xe arc lamp filtered by a 40% transmitting neutral density filter. The light transmitted through the sample was passed through an Instrument SA model LH290 1200 g/mm monochromator and focused onto a photodiode detector. The output was then amplified using a home-built amplifier and fed to a Tektronix digital oscilloscope model TDS 620A for signal averaging. Each transient profile consists of an average of 2000 scans (spectra are shown in Figure S16). The excitation wavelengths were as follow: 623 nm for **5**, 605 nm for **12**, 646 for **18**, 645 nm for **10**, 675 nm for **15**, 500 nm for **17**, 646 nm for **16a** and 650 nm for **16b**.

EPR Spectroscopy

Approximately 1 mg of each sample was dissolved in 1 mL of the solvents listed in Table 1 (toluene - Fisher HPLC grade; pyridine - J.T. Baker 99.9%). All samples were degassed before the experiments by subjecting them to at least 6 freeze-pump-thaw cycles. The EPR experiments were performed at ~20 K using a Bruker EMX X-band spectrometer equipped with ESR 900 continuous helium cryostat and Oxford ICT4 temperature controller. The samples were excited with white light from a 1000 W Xe arc lamp (Kratos LH151N/1S) filtered by a 5 cm layer of water and focused onto the cavity by a set of lenses. For all the spectra, the following instrument settings were used: microwave frequency, 9.4 GHz; modulation frequency, 100 kHz; center field, 3337 G; sweep width, 1000 G; time constant,

328 ms; conversion time, 328 ms; field resolution, 2048 points; number of scans, 8. The light minus dark difference spectra were obtained by subtraction, using Galactic DataMax 2.2 software.

3,7,8,12,13,17,18-Heptaethyl-2a-methyl-2-oxo-2a-homoporphyrin (12)—To a solution of 2,3,7,8,12,13,17,18-octaethyl-2,3-dihydroxychlorin **10** (52 mg, 9.0×10^{-5} mol) in $CHCl_3$ (20 mL) and DBU (1 mL) was added silica-bound $NaIO_4$ (250 mg). The reaction mixture was stirred for 12 h at ambient temperature and monitored by TLC and UV/Vis until most to all of the starting material was consumed (R_f of **10** (silica-$CHCl_3$/3 % MeOH) = 0.31). If necessary, more oxidant was added. Upon consumption of the starting material, the mixture was filtered to remove the silica, washed repeatedly with water and dried over Na_2SO_4. The solvent was removed *in vacuo* and the residue was purified by preparative TLC (500 μm silica, $CHCl_3$/1% MeOH) and recrystallized by slow solvent exchange of CH_2Cl_2 to EtOH to provide **12** as a purple solid (28 mg, 0.05 mmol, 55 %). The reaction is amenable to 10-fold scaling. R_f (silica-$CHCl_3$/3 % MeOH) = 0.50; 1H NMR (500 MHz, [D_1]$CHCl_3$, 25 °C, TMS); δ = 11.03 (s, 1H, 20-CH), 9.78 (s, 1H, 5-CH), 9.62 (s, 1H, 15-CH), 9.56 (s, 1H, 10-CH), 4.13 (m, 4H, 13^1,18^1-CH_2), 4.01 (m, 2H, 17^1-CH_2), 3.90 (m, 2H, 7^1-CH_2), 3.81 (m, 2H, 12^1-CH_2), 3.75 (m, 2H, 8^1-CH_2), 3.71 (m, 2H, 3^1-CH_2), 2.82 (s, 3H, $2a^1$-CH_3), 1.83 (m, 21H, 3^1,7^1,8^1,12^1,13^1,17^1,18^1-CH_3), −3.63 (s, 1H, exchangeable with D_2O, NH,), −3.84 ppm (s, 1H, exchangeable with D_2O, NH,); ^{13}C NMR (125 MHz, [D_1]$CHCl_3$, 25 °C, TMS): δ = 185.9 (2-C=O), 155.0 (11-C), 154.3 (6-C), 152.8 (3-C), 144.8 (12-C), 144.6 (13-C), 143.1 (18-C), 141.7 (14-C), 141.2 (7-C), 138.4 (16,17-C), 138.1, 137.9 (1-C, 4-C), 137.5 (C8), 137.1 (2a-C), 134.0 (19-C), 132.8 (9-C), 103.5 (20-CH), 103.2 (5-CH), 96.2 (10-CH), 95.9 (15-CH), 25.9 (3^1-CH_2), 19.7, 19.6, 19.5, 19.4 (7^1,8^1,12^1,13^1,17^1,18^1-CH_2), 18.5, 18.4, 18.2, 18.1 (7^1,8^1,12^1,13^1,17^1,18^1-CH_3), 16.0 (3^1-CH_3), 12.4 ppm ($2a^1$-CH_3); UV/Vis (CH_2Cl_2): λ_{max} (log ε) = 339 (sh), 424 (5.14), 443 (4.82), 547 (3.80), 587 (4.36), 609 (4.21), 662 nm (3.05); UV/Vis [$CHCl_3$-5% TFA, λ_{max} (log ε)]: 434 (5.29), 546 (3.3), 587 (4.04), 638 (4.24); MS (ESI, cone voltage 30 eV, 100% CH_3CN): *m/z*: 549.4 $[M+H]^+$; HRMS (ESI+, 100% CH_3CN): *m/z* calcd for $C_{36}H_{44}N_4O$: 549.3593, found 549.3589; elemental analysis calcd (%) for $C_{36}H_{44}N_4O$: C, 78.79; H, 8.08; N, 10.21; O, 2.92; found: C, 78.33; H, 8.05; N, 10.00; O, 3.20.

[3,7,8,12,13,17,18-Heptaethyl-2a-methyl-2-oxo-2a-homoporphyrinato]zinc(II) (12Zn)—Zn(II) acetate (40 mg) was added to a solution of **12** (50 mg, 9.0×10^{-5} mol) in $CHCl_3$/10% MeOH (20 mL). The reaction mixture was heated to reflux until the starting material was exhausted, as monitored by TLC and UV/Vis (~30 min). The solvent was removed *in vacuo*, the residue dissolved in $CHCl_3$, washed several times with water, and dried over Na_2SO_4. Crystallization by solvent exchange from $CHCl_3$ to EtOH on the rotary evaporator, followed by filtration, provided **12Zn** as a purple solid in 67% yield (35 mg, 6.0×10^{-5} mol). R_f (silica-$CHCl_3$/5% MeOH) = 0.50; ^1H NMR (400 MHz, 1:1 [D_6]DMSO: [D_4]MeOH, 25 °C, TMS): δ = 10.78 (s, 1H, *meso*-H), 10.09 (s, 1H, *meso*-H), 9.82 (s, 2H, *meso*-H), 3.99 (m, 14H, CH_2CH_3), 2.80 (s, 3H, CH_3), 1.91, 1.81 ppm (m, 21H, CH_2CH_3); ^{13}C NMR (100 MHz, [D_1]$CHCl_3$, 25 °C, TMS): δ = 183.9, 152.6, 149.8, 149.6, 148.8, 148.7, 146.9, 145.8, 144.4, 144.2, 143.4, 143.3, 142.7 142.2, 140.3, 136.7, 135.7, 103.0, 102.6, 97.8, 97.7, 31.2, 26.3, 19.7, 19.5, 19.4, 19.2, 19.1, 19.0, 16.8, 13.0 ppm; UV/Vis ($CHCl_3$): λ_{max} (log ε) = 434 (4.64), 453 (4.36), 578 (3.45), 627 nm (3.83); MS (ESI+, cone voltage 30 eV, 100% CH_3CN): *m/z* 611.1 $[M+H]^+$; HRMS (EI): *m/z* calcd for $C_{36}H_{42}N_4O$: 549.3593, found 549.3589.

3,7,8,12,13,17,18-Heptaethyl-2a-hydro-3-hydroxy-2a-methyl-2-oxo-2a-homoporphyrin (14)—R_f (silica-$CHCl_3$) 0.21; ^1H NMR (400 MHz, [D_1]$CHCl_3$, 25 °C, TMS): δ = 10.46 (s, 1H), 9.94 (s, 1H), 9.88 (s, 1H), 9.80 (s, 1H), 4.08 (m, 8H), 3.90 (m, 4H), 3.63 (m,

4H), 2.97 (m, 3H), 1.84 (m, 21H), −3.59, −3.79 ppm (s, 2H, NH): ^{13}C NMR (100 MHz, [D_1]$CHCl_3$, 25 °C, TMS): δ = 202.1, 154.1, 153.1, 151.3, 144.5, 143.5, 139.81, 139.4, 138.3, 137.0, 135.7, 135.3, 134.3, 132.5, 98.8, 98.0, 97.9, 96.6, 79.7, 70.6, 51.6, 45.7, 42.2, 32.3, 19.7, 19.6, 19.6, 19.5, 19.1, 18.6, 18.5, 18.4, 18.3, 18.2, 18.1, 13.7, 12.3, 11.2, 8.5, 8.1 ppm; UV/Vis (CH_2Cl_2): λ_{max} (rel. int.) = 410 (1.00), 493 (0.05), 512 (0.05), 555 (0.08), 589 (0.05), 645 nm (0.12); MS (ESI+, cone voltage 30 eV, 100% CH_3CN): *m/z*: 567.6 $[M+1]^+$; HRMS (EI): *m*/*e* calcd for $C_{36}H_{46}N_4O_2$: 567.3699, found 567.3679.

3,7,8,12,13,17,18-Heptaethyl-12,13-dihydroxy-2a-methyl-2-oxo-2a-homochlorin (15)—In a single neck round bottom flask, oxypyriporphyrin **12** (55 mg, 9.8×10^{-5} mol) is dissolved in a 2:3 mixture (15 mL) of $CHCl_3$ (EtOH-stabilized) and pyridine (distilled from $KMnO_4$). To this are added 25 mg OsO_4 (1.25 mL of a stock solution of 0.1 g OsO_4 in 5 mL pyridine). CAUTION: Fume hood and eye protection! The flask is stoppered and protected from light (aluminum foil) and stirred for 7 d at ambient temperature. The osmate ester of **15** forms as the only polar, green product. After this time, gaseous H_2S is bubbled through the solution for 1 min. The mixture is stirred for 30 min and TLC control should confirm the conversion of the new compound into a slightly more polar product of the same color and UV/Vis spectrum. The mixture is then filtered through a pad of Celite (diatomaceous earth) and is evaporated to dryness on the rotary evaporator. Preparative plate or column chromatography (silica-CH_2Cl_2), followed by recrystallization by slow solvent exchange from $CHCl_3$ to EtOH on the rotary evaporator yielded **15** as a green powder (40 mg, 68% yield). Alternatively, the compound can be isolated in varying yields as an intermediate product during the MnO_4–-oxidation of tetraolbacteriochlorin **17**, see below. R_f (silica-$CHCl_3$/1 % MeOH) = 0.25; ^{1}H NMR (400 MHz, [D_1]$CHCl_3$, 25 °C, TMS): δ = 9.22 (s, 1H, 5-H), 8.94 (s, 1H, 20-H), 8.71 (s, 1H, 10-H), 8.32 (s, 1H, 15-H), 5.52 (br s, 1H, exchangeable with D_2O, OH), 5.31 (br s, 1H, exchangeable with D_2O, OH), 3.84 (m, 4H, 7^1,8^1-CH_2), 3.53 (m, 2H, 3^1-CH_2), 3.28 (m, 1H, 17^1-CH_2), 3.01 (m, 1H, 17^1-CH_2), 2.73 (m, 2H, 18^1-CH_2), 2.58 (s, 3H, $2a^1$-CH_3), 2.47 (4H, m, 12^1,13^1-CH_2), 1.78 (t, ^3J = 8 Hz, 3H, 7^1-CH_3), 1.76 (t, ^3J = 8 Hz, 3H, 8^1-CH_3), 1.62 (t, ^3J = 7 Hz, 3H, 3^1-CH_3), 1.37 (t, ^3J = 7 Hz, 3H, 17^1-CH_3), 1.13 (t, ^3J = 7 Hz, 3H, 18^1-CH_3), 1.07 (t, ^3J = 7 Hz, 6H, 12^1,13^1-CH_3) −2.55, −3.23 ppm (s, 2H, exchangeable with D_2O, NH); ^{13}C NMR (125 MHz, [D_1]$CHCl_3$, 25 °C, TMS): δ = 181.5 (2-C=O), 151.2 (3-C), 143.6, 142.4, 141.4, 139.1, 135.2, 135.0, 134.5 (1,4,6,7,8,9,11,14,16,17,18,19-C), 135.6 (2a-C), 105.5 (5,20-C), 92.2 (10-C), 92.0 (15-C), 85.1, 84.9 (12,13-C), 28.4, 28.2 (12^1,13^1-CH_2), 25.6 (3^1-CH_2), 19.7, 19.2, 18.0, 17.9, 17.6, 17.2, 16.0 (3^1,7^1,8^1,17^1,18^1-CH_3, 7^1,8^1,17^1,18^1-CH_2), 12.4 ($2a^1$-CH_3), 8.50, 8.46 ppm (12^1,13^1-CH_3); UV/Vis ($CHCl_3$): λ_{max} (log ε) = 402 (3.86), 426 (4.57), 449 (4.03), 541 (4.12), 575 (sh), 587 (3.48), 613 (3.46), 668 nm (3.52); MS (ESI+, 30 V cone voltage, 100% CH_3CN): *m/z*: 583.2 $[M+H]^+$; HRMS (ESI+, 30 V cone voltage, 100% CH_3CN): *m/z* calcd for $C_{36}H_{47}N_4O_3$: 583.3643, found 583.3644.

3,7,8,12,17,18-Hexaethyl-2a,13a-dimethyl-2,13-dioxo-2a,12a-homoporphyrin (16a) and 3,7,8,13,17,18-hexaethyl-2a,12a-dimethyl-2,12-dioxo-2a,12a-homo-porphyrin (16b)—To a solution of 2,3,7,8,12,13,17,18-octaethyl-2,3,12,13-tetrahydroxybacteriochlorin (**17**, isomerically pure or mixture of the two possible stereoisomers) (50 mg, 8.3×10^{-5} mol) in $CHCl_3$ (50 mL) and DBU (1.0 mL) were added the silica-bound $NaIO_4$ (250 mg). The reaction mixture was stirred for ~2 h until all the starting material was consumed (monitored by TLC – R_f of **17** (silica-$CHCl_3$/5% MeOH) = 0.15 – and UV/Vis spectroscopy – reduction of the band at λ = 709 nm). The mixture was filtered to remove the silica gel and washed with water, 1% aq HCl, water, and dried over Na_2SO_4. The solvent was removed *in vacuo*. The residue was separated and purified by preparative TLC (500 μm silica, CH_2Cl_2). The two major dark-green bands were isolated and recrystallized by slow solvent exchange from CH_2Cl_2 to MeOH to provide the two

isomeric bis(oxypyri)porphyrins **16a** and **16b** (each 11 mg, 2.1×10^{-5} mol, 25%) as purple solids. An additional product, appearing in varying yields, could be identified as **15**. Alternatively, dihydroxy-oxypyriporphyrin **15** could be, using the identical methodology, oxidized to provide **16a** and **16b** in 35% yields each.

16a: R_f (silica-$CHCl_3$/1 % MeOH) = 0.34; ^{1}H NMR (500 MHz, [D_1]$CHCl_3$, 25 °C, TMS): δ = 10.44 (s, 2H, 15,20-H), 9.41 (s, 2H, 5,10-H), 3.99 (q, ^3J = 8 Hz, 4H, 17^1,18^1-CH_2), 3.73 (q, ^3J = 8 Hz, 4H, 7^1,8^1-CH_2), 3.68 (q, ^3J = 8 Hz, 4H, 3^1,12^1-CH_2), 2.72 (s, 6H, $2a^1$,$12a^1$-CH_3), 1.78 (t, ^3J = 8 Hz, 6H, 17^1,18^1-CH_3), 1.74 (t, ^3J = 8 Hz, 6H, 3^1,12^1-CH_3), 1.66 (t, ^3J = 8 Hz, 6H, 7^1,8^1-CH_3), −4.35 (s, 1H, NH), −4.40 ppm (s, 1H, NH); ^{13}C NMR (125 MHz, [D_1]$CHCl_3$, 25 °C, TMS): δ = 185.6 (2,13-C=O), 152.5 (3,12-C), 142.7 (1,14-C), 142.3 (17,18-C), 140.3 (7,8-C), 139.5 (4,11-C), 137.4 (2a,12a-C), 136.4 (16,19-C), 134.6 (6,9-C), 103.2 (5,10-CH), 102.4 (15,20-CH), 25.7 (3^1,12^1-CH_2), 19.6 (7^1,8^1,17^1,18^1-CH_2) 18.0 (17^1,18^1-CH_3), 17.8 (7^1,8^1-CH_3), 15.6 (3^1,12^1-CH_3), 12.2 ppm ($2a^1$,$12a^1$-CH_3); UV/Vis ($CHCl_3$): λ_{max} (log ε) = 408 (sh), 435 (5.19), 465 (4.80), 578 (3.82), 624 (4.58), 652 (4.51), 708 nm (3.39); MS (ESI+, cone voltage 30 eV, 100% CH_3CN): *m/z*: 563.3 $[M+H]^+$, HRMS (ESI+) *m/z* calcd for $C_{36}H_{43}N_4O_2$: 563.3381, found 563.3366.

16b: R_f (silica-$CHCl_3$/1% MeOH) = 0.43; ^{1}H NMR (400 MHz, [D_1]$CHCl_3$, 25 °C, TMS): δ = 10.55 (s, 2H, 10,20-H), 9.72 (s, 2H, 5,15-H), 3.99 (q, ^3J = 8 Hz, 4H, 8^1,18^1-CH_2), 3.92 (q, ^3J = 8 Hz, 4H, 7^1,17^1-CH_2), 3.81 (q, ^3J = 8 Hz, 4H, 3^1,13^1-CH_2), 2.74 (s, 6H, $2a^1$,$12a^1$-CH_3), 1.83 (t, ^3J = 8 Hz, 6H, 3^1,13^1-CH_3), 1.79 (m, 12H, 7^1,8^1,17^1,18^1-CH_3), −3.80 ppm (s, 2H, NH); ^{13}C NMR (100 MHz, [D_1]$CHCl_3$, 25 °C, TMS): δ = 186.0 (2,12-C=O), 152.4 (3,13-C), 142.3 142.1, 140.7, 140.4, 135.8, 135.6 (1,4,6,9,11,14,16,19-C), 137.6 (2a-C, 12a-C), 103.2, 102.9 (5,10,15,20-CH), 25.7 (3^1,13^1-CH_2), 19.7, 19.6 (7^1,8^1,17^1,18^1-CH_2), 18.3, 17.8 (7^1,8^1,17^1,18^1-CH_3), 15.7 (3^1,13^1-CH_3), 12.2 ppm ($2a^1$,$12a^1$-CH_3); UV/Vis ($CHCl_3$): λ_{max} (log ε) = 435 (5.05), 464 (4.83), 578 (3.71), 625 (4.40), 655 (4.32), 710 nm (3.48); MS (ESI+, cone voltage 30 eV, 100% CH_3CN): *m/z*: 563.1 $[M+H]^+$; HRMS (ESI+): *m/z* calcd for $C_{36}H_{43}N_4O_2$: 563.3381, found 563.3359.

X-ray Crystallography

Single crystals (black plates) of **12** were grown upon slow evaporation of MeOH/CH_2Cl_2 solutions to dryness.

Diffraction data of a 0.34 × 0.33 × 0.04 mm crystal were collected on a Bruker AXS SMART APEX CCD diffractometer with an Apex2 software upgrade at 100(2) K using monochromatic Mo Kα radiation (λ = 0.71073 Å) using the ω scan technique. The data were collected using SMART, and the data integration and unit cell determination was made using Apex2; the sadabs multi-scan absorption correction as embedded in Apex2 was applied.[58] The structure was solved by direct methods and refined by full matrix least squares against F^2 against all reflections using SHELXTL.[58] A full-matrix refinement method on the least-squares on F^2 was applied.[58] Non-hydrogen atoms were refined with anisotropic displacement parameters. All hydrogen atoms were placed in calculated positions and were isotropically refined with a displacement parameter of 1.2 times that of the adjacent carbon atom. The refinement converged satisfactorily. Crystal structure and refinement data for **12** are summarized in Table 2.

The molecule exhibits whole molecule disorder with an occupancy rate for the major moiety of 0.567(2). Equivalent disordered sections of the molecule were restrained to have similar geometries and a global restraint (DELU restraint as described in SHELXTL)[58] was applied to ensure that anisotropic displacement parameters of spatially nearby atoms are similar. For the atom pairs C36 and C31b, C31 and C36b, C24 and C24b, C25 and C25b,

C35 and C30b, and C30 and C35b the anisotropic displacement parameters were constrained to be identical.[59] Atoms C24 and C25 were restrained to be close to isotropic.

Supplementary Material

Refer to Web version on PubMed Central for supplementary material.

Acknowledgments

We thank Professor David Dolphin, University of British Columbia, Vancouver, Canada, for a generous gift of octaethylporphyrin and Pedro Daddario for editorial assistance. This work was supported by the US National Science Foundation under Grant Numbers CHEM-0517782 and CCMI-0730826 (to CB). NLM acknowledges an NSF REU fellowship. This work is supported in the laboratory of HAF by the National Institute of Health (GM-30353) and the University of Connecticut Research Foundation. The diffractometer was funded by NSF grant 0087210, by Ohio Board of Regents grant CAP-491, and by YSU.

References

1. Scheer, H. Chlorophylls. CRC; Boca Raton: 1991.
2. (a) Jentzen W, Ma JG, Shelnutt JA. Biophys J. 1998; 74:753. [PubMed: 9533688] (b) Ma JG, Laberge M, Song XZ, Jentzen W, Jia SL, Zhang J, Vanderkooi JM, Shelnutt JA. Biochemistry. 1998; 37:118.(c) Shelnutt JA, Song XZ, Ma JG, Jentzen W, Medforth CJ. Chem Soc Rev. 1998; 27:31.
3. (a) Kadish, KM.; Smith, KM.; Guilard, R., editors. The Porphyrin Handbook. Vol. 1–10. Academic Press; San Diego: 2000. (b) Kadish, KM.; Smith, KM.; Guilard, R., editors. The Porphyrin Handbook. Vol. 11–20. Academic Press; San Diego: 2003.
4. For recent examples, see: Muthiah C, Bhaumik J, Lindsey JS. J Org Chem. 2007; 72:5839. [PubMed: 17585826] Ptaszek M, McDowell BE, Taniguchi M, Kim HJ, Lindsey JS. Tetrahedron. 2007; 63:3826. [PubMed: 17479168] Taniguchi M, Ptaszek M, McDowell BE, Lindsey JS. Tetrahedron. 2007; 63:3840. [PubMed: 17479170] Taniguchi M, Ptaszek M, McDowell BE, Boyle PD, Lindsey JS. Tetrahedron. 2007; 63:3850. [PubMed: 17479169] O'Neal WG, Jacobi PA. J Am Chem Soc. 2008; 130:1102. [PubMed: 18166060] Borbas KE, Ruzié C, Lindsey JS. Org Lett. 2008; 10:1931. [PubMed: 18422289] Muthiah C, Ptaszek M, Nguyen TM, Flack KM, Lindsey JS. J Org Chem. 2007; 72:7736. [PubMed: 17803319] Ruzié C, Krayer M, Balasubramanian T, Lindsey JS. J Org Chem. 2008; 73:5806. and references therein. [PubMed: 18576691]
5. (a) Asat A, Dolphin D. Chem Rev. 1997; 97:2267. [PubMed: 11848901] (b) Sessler, JL.; Weghorn, S. Expanded, Contracted & Isomeric Porphyrins. Pergamon; New York: 1997. (c) Sessler, JL.; Gebauer, A.; Weghorn, SJ. The Porphyrin Handbook. Kadish, KM.; Smith, KM.; Guilard, R., editors. Vol. 2. 2000. p. 55(d) Maeda H, Furuta H. Pure Appl Chem. 2006; 78:29.(e) Srinivasan A, Furuta H. Acc Chem Res. 2005; 38:10. [PubMed: 15654732]
6. (a) Lash, TD. The Porphyrin Handbook. Kadish, KM.; Smith, KM.; Guilard, R., editors. Vol. 2. Academic Press; San Diego: 2000. p. 125(b) Lash TD. J Porphyrins Phthalocyanines. 2001; 5:267. (c) Lash TD. Eur J Org Chem. 2007:5461.
7. Lash TD. Synlett. 2000:279.
8. Berlin K, Breitmaier E. Angew Chem, Int Ed Engl. 1994; 33:1246.
9. Mysliborsky R, Latos-Grazynski L, Szterenberg L. Eur J Org Chem. 2006:3046.
10. Berlin K, Breitmaier E. Angew Chem, Int Ed Engl. 1994; 33:219.
11. Callot HJ, Schaeffer E. Tetrahedron. 1978; 34:2295.
12. Lash TD, Pokharel K, Serling JM, Yant VR, Ferrence GM. Org Lett. 2007; 9:2863. [PubMed: 17602489]
13. Schönemeier T, Breitmaier E. Synthesis. 1997:273.
14. (a) Lash TD. Angew Chem; Int Ed Engl. 1995; 34:2533.(b) Lash TD, Chaney ST. Chem—Eur J. 1996; 2:944.
15. Lash TD, Chaney ST, Richter DT. J Org Chem. 1998; 63:9076.
16. Liu D, Ferrence GM, Lash TD. J Org Chem. 2004; 69:6079. [PubMed: 15373493]

17. Eguchi H, Ohgo Y, Ikezaki A, Neya S, Nakamura M. Chem Lett. 2008; 37:768.
18. Neya S, Suzuki M, Ode H, Hoshino T, Furutani Yuji, Kandori H, Hori H, Imai K, Komatsu T. Inorg Chem. 2008; 47:10771. [PubMed: 18844346]
19. Callot HJ. Dalton Trans. 2008:6346. [PubMed: 19002318]
20. Crossley MJ, King LG. J Chem Soc, Chem Commun. 1984:920.
21. (a) Campbell CJ, Rusling JF, Brückner C. J Am Chem Soc. 2000; 122:6679.(b) Daniell HW, Brückner C. Angew Chem, Int Ed. 2004; 43:1688.(c) McCarthy JR, Hyland MA, Brückner C. Org Biomol Chem. 2004; 2:1484. [PubMed: 15136804] (d) Lara KK, Rinaldo CK, Brückner C. Tetrahedron. 2005; 61:2529.(e) Perez MJ, McCarthy JR, Brückner C, Weissleder R. Nano Lett. 2005; 5:2552. [PubMed: 16351214]
22. (a) Crossley MJ, Burn PL, Langford SJ, Pyke SM, Stark AG. J Chem Soc, Chem Commun. 1991:1567.(b) Crossley MJ, Burn PL, Chew SS, Cuttance FB, Newsom IA. J Chem Soc, Chem Commun. 1991:1564.(c) Starnes SD, Rudkevich DM, Rebek J Jr. J Am Chem Soc. 2001; 123:4659. [PubMed: 11457274] (d) Daniell HW, Williams SC, Jenkins HA, Brückner C. Tetrahedron Lett. 2003; 44:4045.
23. Kozyrev AN, Alderfer JL, Dougherty TJ, Pandey RK. Angew Chem; Int Ed Engl. 1999; 38:126.
24. One other example of a bis-pyrrole-modified porphyrinoid is a bis-carbaporphyrin: Graham SR, Colby DA, Lash TD. Angew Chem Int Ed Engl. 2002; 41:1371. [PubMed: 19750768]
25. Brückner C, Rettig SJ, Dolphin D. J Org Chem. 1998; 63:2094.
26. (a) Bonnett R, Dimsdale MJ, Stephenson GF. J Chem Soc C. 1969:564.(b) Chang CG, Sotiriou C. J Heterocyclic Chem. 1985; 22:1739.(c) Adams KR, the late Berenbaum MC, Bonnett R, Nizhnik AN, Salgado A, Asunción Vallés M. J Chem Soc, Perkin Trans. 1992; 1:1465.
27. Adams KR, Bonnett R, Burke PJ, Salgado A, Vallés MA. J Chem Soc, Chem Commun. 1993:1860.
28. Adams KR, Bonnett R, Burke PJ, Salgado A, Vallés MA. J Chem Soc, Perkin. 1997; 1:1769.
29. Lash TD, Chaney ST. Chem Eur J. 1996; 2:944.
30. (a) Brückner C, Sternberg ED, MacAlpine JK, Rettig SJ, Dolphin D. J Am Chem Soc. 1999; 121:2609.(b) Brückner C, Hyland MA, Sternberg ED, MacAlpine J, Rettig SJ, Patrick BO, Dolphin D. Inorg Chim Acta. 2005; 358:2943.
31. McCarthy JR, Melfi PJ, Capetta SH, Brückner C. Tetrahedron. 2003; 59:9137.
32. McCarthy JR, Jenkins HA, Brückner C. Org Lett. 2003; 5:19. [PubMed: 12509880]
33. Ketone-functionalized zinc chlorins have been designed to form Lewis-acid (zinc center)-Lewis base (ketone functionality) coordination aggregates, thus this behavior does not surprise. See, e.g.: Balaban TS. Acc Chem Res. 2005; 38:612. [PubMed: 16104684]
34. Note the difference of the conformation of **2** compared to the carbaporphyrin isomers of pyriporphyrins, see, e.g. ref. 12.
35. CCSD code OETPOR10. Lauher JW, Ibers JA. J Am Chem Soc. 1973; 95:5148. [PubMed: 4733806]
36. Kolb HC, Van Nieuwenhze MS, Sharpless KB. Chem Rev. 1994; 94:2483.
37. Whitlock HW Jr, Hanamer R, Oester MY, Bower BK. J Am Chem Soc. 1969; 91:7485.
38. Chang CG, Sotiriou C, Weishih W. J Chem Soc, Chem Comm. 1986:1213.
39. a) Pandey RK, Shiau FY, Isaac M, Ramaprasad S, Dougherty TJ, Smith KM. Tetrahedron Lett. 1992; 33:7815.b) Smith KM, Goff DA. J Am Chem Soc. 1985; 107:4954.c) Brückner C, Dolphin D. Tetrahedron Lett. 1995; 36:9425.
40. Meunier I, Pandey RK, Walker MM, Senge MO, Dougherty MTJ, Smith KM. Bioorg Med Chem Lett. 1992; 2:1575.
41. Pandey RK, Isaac M, MacDonald I, Medforth CJ, Senge MO, Dougherty TJ, Smith KM. J Org Chem. 1997; 62:1463.
42. Knyukshto V, Zenkevich E, Sagun E, Shulga A, Bachilo S. Chem Phys Lett. 1998; 297:97.
43. Turro, NJ. Modern Molecular Photochemistry. University Science Books; California: 1991.
44. Brückner C, McCarthy JR, Daniell HW, Pendon ZD, Ilagan RP, Francis TM, Ren L, Birge RR, Frank HA. Chem Phys. 2003; 294:285.

45. Carrington, A.; McLachlan, AD. Introduction to Magnetic Resonance. Harper and Row; New York: 1967.
46. Weil, JA.; Bolton, JR.; Wertz, JE. Electron Paramagnetic Resonance. Wiley and Sons; New York: 1994.
47. Welter, W. Magnetic Atoms and Molecules. Dover Publications; New York: 1989.
48. Angiolillo PJ, Lin VSY, Vanderkooi JM, Therien MJ. J Am Chem Soc. 1995; 117:12514.
49. Hamacher V, Wrachtrap J, von Maltzan B, Plato M, Pöbius K. Appl Magnetic Resonance. 1993; 4:297.
50. Kleibeuker JF, Schaafsma TJ. Chem Phys Lett. 1974; 29:116.
51. Shediac R, Gray MHB, Uyeda HT, Johnson RC, Hupp JT, Angiolillo PJ, Therien MJ. J Am Chem Soc. 2000; 122:7017.
52. Ponte Goncalves AM, Burgner RP. J Chem Phys. 1976; 65:1221.
53. (a) McCarthy JR, Melfi PJ, Capetta SH, Brückner C. Tetrahedron. 2003; 59:9137.(b) Lau KSF, Sadilek M, Khalil GE, Gouterman M, Brückner C. J Am Soc Mass Spectrom. 2005; 16:1915. [PubMed: 16246578] (c) Lau KSF, Sadilek M, Khalil GE, Gouterman M, Brückner C. J Am Soc Mass Spectrom. 2006; 17:1306. [PubMed: 16857382]
54. (a) Berkel GJV, McLuckey SA, Glish GL. Anal Chem. 1991; 63:1098.(b) Domingues MRM, Domingues P, Reis A, Ferrer-Correira AJ, Tomé JPC, Tomé AC, Neves MGPMS, Cavaleiro JAS. J Mass Spectrom. 2004; 39:158. [PubMed: 14991685] (c) Domingues MRM, Marques MGOS, Domingues P, Graça Neves M, Cavaleiro JAS, Ferrer-Correia AJ. Am Soc Mass Spectrom. 2001; 12:381.(d) Izquerido RA, Barros CM, Santana-Marques MG, Correia AJF, Silva AMG, Tome AC, Silva A, Neves MGPMS, Cavaleiro JAS. Rapid Commun Mass Spectrom. 2004; 18:2601. [PubMed: 15476189] (e) Quirke, JME. The Porphyrin Handbook. Kadish, KM.; Smith, KM.; Guilard, R., editors. Vol. 7. Academic Press; San Diego: 2000. p. 371(f) Silva EMP, Domingues MRM, Barros C, Faustino MAF, Tomé JPC, Neves MGPMS, Tomé AC, Santana-Marques MG, Cavaleiro JAS, Ferrer-Correia AJ. J Mass Spectrom. 2005; 40:117. [PubMed: 15643640] (g) Van Berkel GJ, McLuckey SA, Glish GL. Anal Chem. 1991; 63:1098.
55. Callot HJ, Johnson AW. J Chem Soc; Chem Commun. 1969:749.
56. Sessler JL, Mozaffari A, Johnson MR. Org Syn. 1992; 70:68.
57. Zhong YL, Shing TKM. J Org Chem. 1997; 62:2622. [PubMed: 11671605]
58. (a) Bruker Advanced X-ray Solutions SMART for WNT/2000 (Version 5.628). Bruker AXS Inc; Madison, WI, USA: 1997–2002. (b) Bruker Advanced X-ray Solutions SAINT (Version 6.45). Bruker AXS Inc; Madison, WI, USA: 1997–2003. (c) Bruker Advanced X-ray Solutions SHELXTL (Version 6.10). Bruker AXS Inc; Madison, WI, USA: 2000.
59. Please note that the numbering system used for **12** in the diffractometry study differs from that used in the NMR studies, see SI for details.

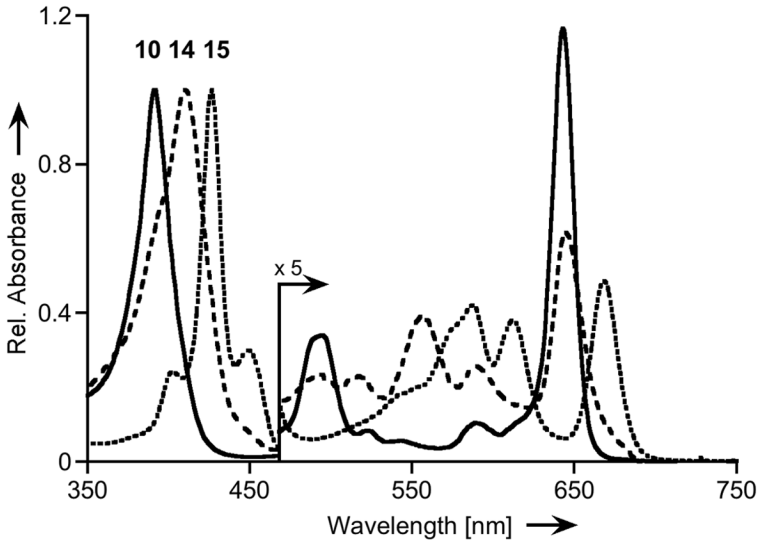

Figure 1.

Normalized UV/Vis spectra ($CHCl_3$) of dihydroxychlorin **10** (solid trace), cleavage product **14** (dashed trace), and 12,13-dihydroxyoxypyriporphyrin **15** (dotted trace).

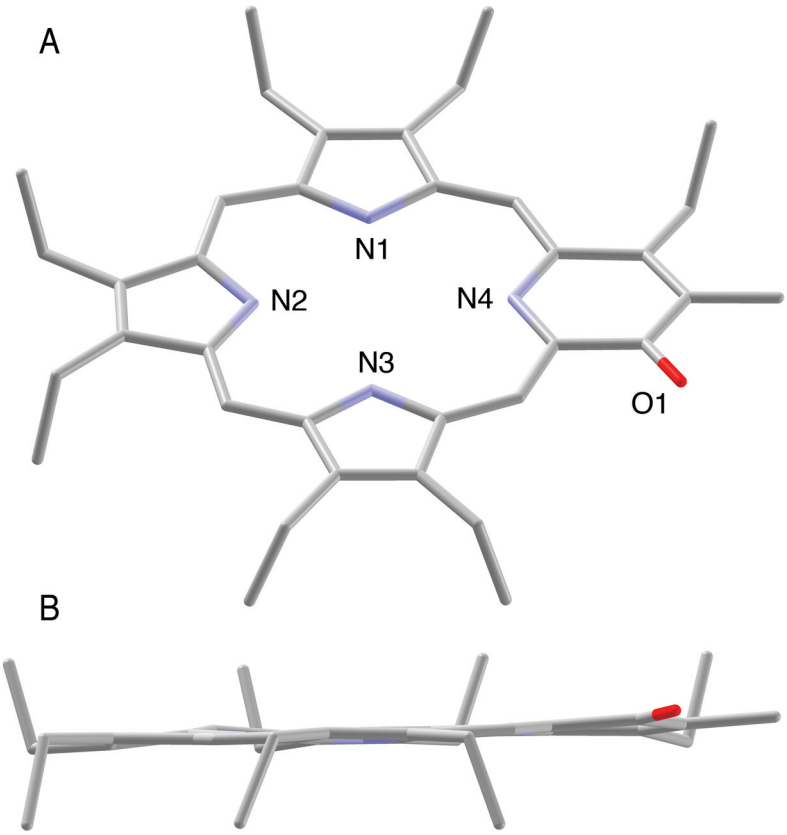

Figure 2.
View of the molecular structure of **12**. Only one of the two whole molecule-disordered molecules is shown. A. View from an oblique angle. B. Side view along the N3-N1 axis, highlighting the degree of planarity of the macrocycle.

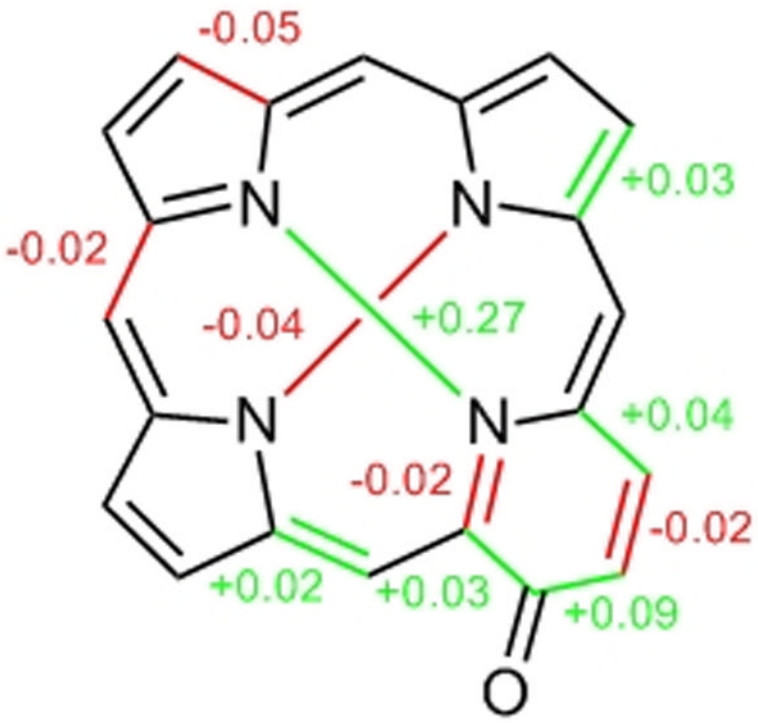

Figure 3.
Differences in bond length (in Å) observed in **12** compared to **5**.[31] Arbitrarily, only differences that are equal or larger than 0.02 Å, i.e. equal or larger than 2 × the average e.s.d. for C-C bond lengths determined for **12** (e.s.d. = 0.01 Å), are considered. Comparison of the distances in the pyridone moiety with those of a pyrrolic moiety in **5** carrying an imine-type nitrogen.

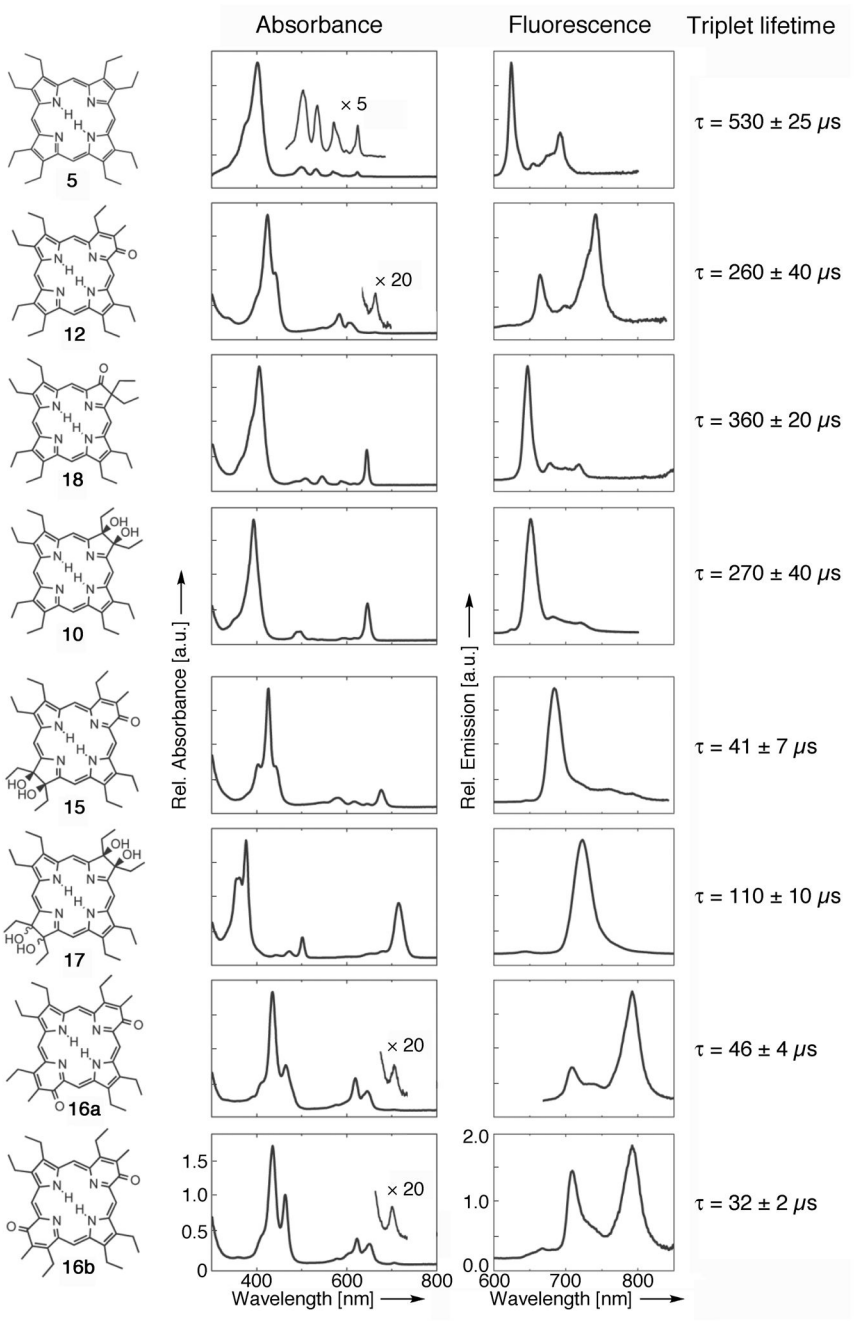

Figure 4.

The normalized absorption and fluorescence emission spectra and triplet life-times of **5**, **12**, **18**, **10**, **15**, **17**, **16a**, and **16b** (all at ambient temperature, degassed toluene). The triplet excited state lifetimes were calculated as mean of at least eight decay constants of the decay kinetics taken (440 nm for **5**, 470 nm for **12**, 470 nm for **18**, 430 nm for **10**, 460 nm for **15**, 420 nm for **17**, 520 nm for **16a** and 510 nm for **16b**). For the transient triplet-triplet absorption spectra, see SI Figure S16.

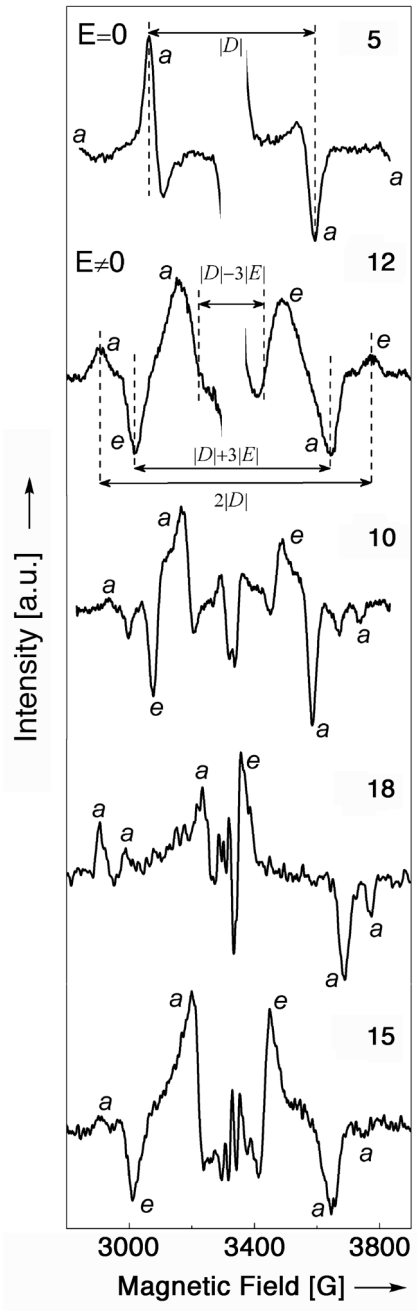

Figure 5.
X-band EPR spectra of the light-induced triplet states, presented as light-minus-dark difference plots of (**5**), (**10**), (**12**), (**15**) and (**18**). The letters *a* and *e* correspond to signals associated with absorption and emission.

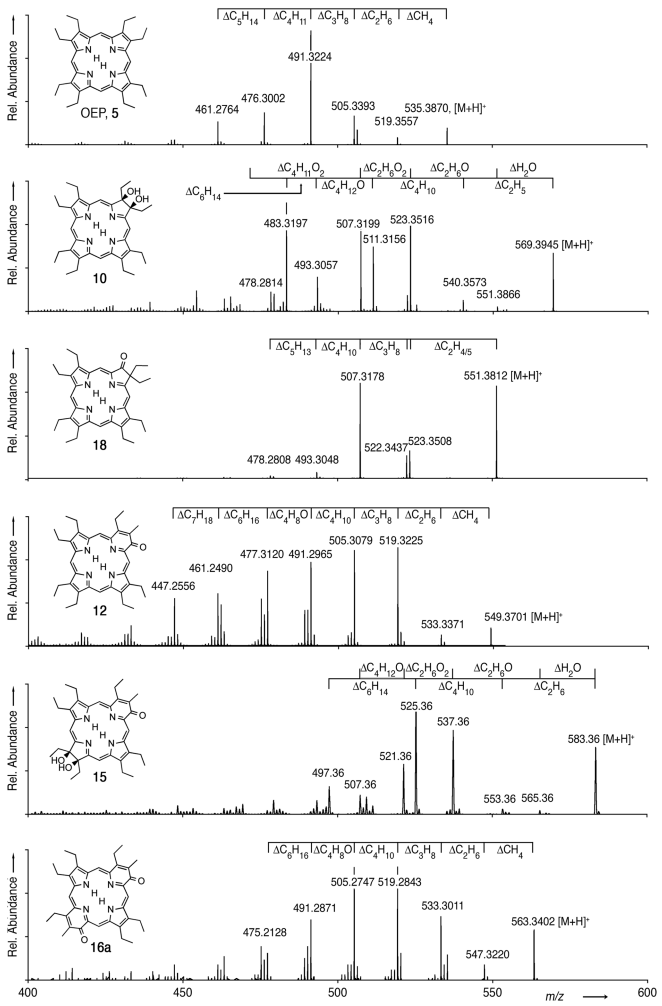

Figure 6.

Collision-induced fragmentation spectra (ESI+, 100% CH_3CN) of **5**, **10**, **12**, **15**, **16a**, and **18**. Except for the spectrum of **15**, all spectra were recorded using a Q-TOF mass spectrometer providing high accuracy data, allowing a direct conclusion on the compositions of the fragment ions. Composition differentials listed are based on $[M+H]^+$.

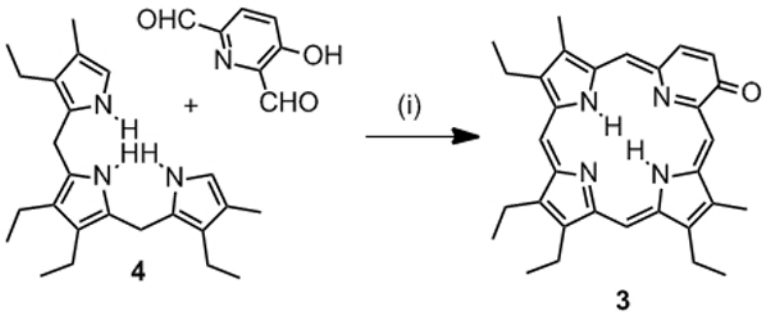

Scheme 1.
3+1 synthesis of oxypyriporphyrin **3**.[15] *Reaction Conditions:* 1. [H^+], 2. DDQ.

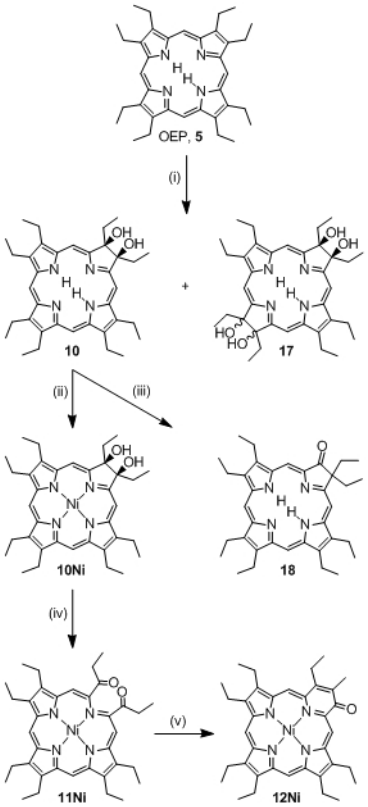

Scheme 2.

Bonnett's synthesis of secochlorin **11Ni**, pyriporphyrin **14Ni**, and the literature-known pathway towards tetraol bacteriochlorin **17** and oxochlorin **18**. *Reaction Conditions:* (i)[25] 1. OsO_4/pyridine, 2. H_2S, 3. chromatographic separation; (ii)[25] Ni(II) acetate, pyridine, Δ; (iii)[26] cat. $HClO_4$, benzene, Δ; (iv)[27,28] Pb(IV) acetate, THF; (v)[27,28] base.

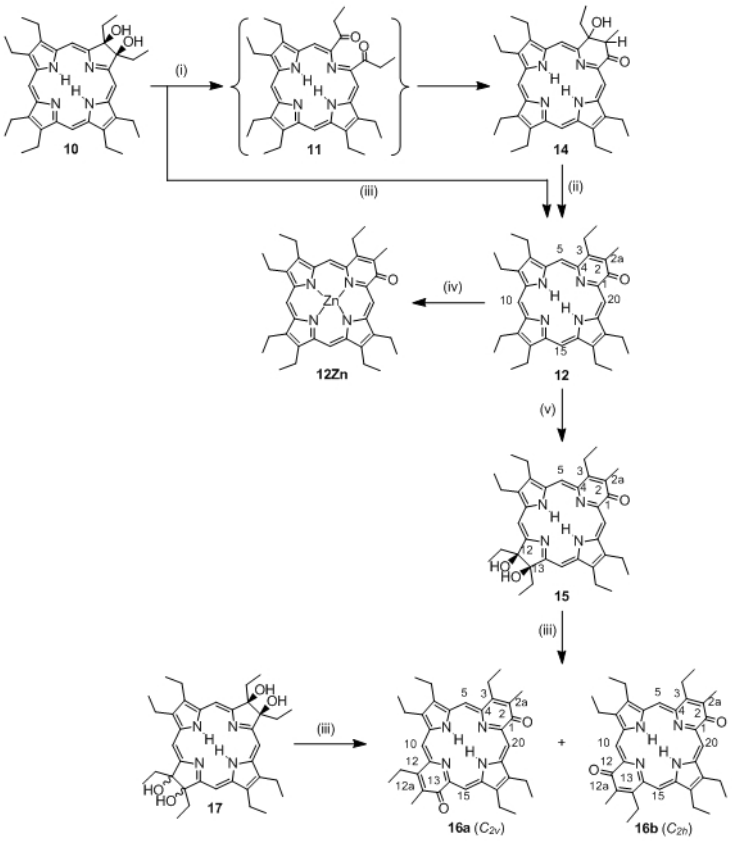

Scheme 3.

Syntheses of the free base chromophores **12**, **14** - **18**. *Reaction Conditions:* (i) 1. $NaIO_4$/silica, Et_3N, $CHCl_3$, 2. chromatographic separation; (ii) cat. acid or base; (iii) 1. $NaIO_4$/silica, DBU, $CHCl_3$, 2. chromatographic separation; (iv) Zn(II) acetate, $CHCl_3$/MeOH, Δ; (v) 1. OsO_4/py, $CHCl_3$ 2. H_2S, 3. chromatographic separation.

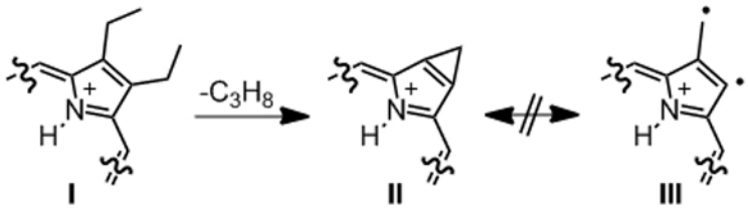

Scheme 4.
Proposed rationalization for the prominent C_3H_8 fragment from β,β′-diethyl-substituted porphyrins.

Table 1

Room temperature triplet state EPR polarization data (white light excitation sources) of the molecules indicated.

Molecule	$\lvert D\rvert$[a] [10^{-4} cm^{-1}]	$\lvert E\rvert$[b] [10^{-4} cm^{-1}]	$\frac{3\lvert E\rvert}{\lvert D\rvert}$ [c]	$\sqrt[3]{\langle r^3\rangle}_d$ [Å]	Polarization pattern
5[e]	495 ± 1	0	0	2.72	*aa/aa*
12[e]	397 ± 10	66 ± 1	0.50	2.93	*aea/eae*
10[e]	370 ± 7	69 ± 1	0.55	3.00	*aea/eaa*
15[f]	393 ± 1	66 ± 1	0.50	2.94	*aea/eaa*
18[e]	399 ± 3	88 ± 1	0.66	2.92	*aaa/eaa*

a,b zero field splitting parameters;

c rhombocity;

d mean inter-electron distance;

e solvent toluene:tyridine 10:1 (v/v); room temperature;

f solvent tyridine

Table 2

Crystal data and refinement details for **12**.

	12
empirical formula	$C_{36}H_{44}N_4O$
M_r	548.75
crystal size [mm]	0.55 × 0.44 × 0.08
crystal system	triclinic
space group	*P*-1 (No. 2)
a [Å]	9.221(3)
b [Å]	13.466(4)
c [Å]	13.493(4)
α [°]	71.062(4)
β [°]	73.391(4)
γ [°]	76.189(4)
V [Å^3]	1498.9(7)
Z	2
$\rho_{calcd.}$ [g cm^{-3}]	1.216
F(000)	592.5
μ [mm^{-1}]	0.074
T_{max}/T_{min}	0.759/0.994
hkl range	±12, ±17, −14 – 17
θ range [°]	2.3355 – 29.232
measured refl.	12464
unique refl. [R_{int}]	7156
observed refl. $I>2\sigma(I)$	2989
refined parameters	655
restraints	292
goodness-of-fit	1.025
*R*1 ($I>2\sigma(I)$)	0.0827
*wR*2 (all data)	0.1876
residual electron density [e Å^{-3}]	−0.220/0.313